Iron abundances of B-type post-asymptotic giant branch stars in globular clusters: Barnard29 in M13 and ROA5701 in Cen

Thompson, H. M. A., Keenan, F. P., Dufton, P. L., Ryans, R. S. I., Smoker, J. V., Lambert, D. L., & Zijlstra, A. A. (2007). Iron abundances of B-type post-asymptotic giant branch stars in globular clusters: Barnard29 in M13 and ROA5701 in Cen. Monthly Notices of the Royal Astronomical Society, 384, 1619-1632. DOI: 10.1111/j.1365-2966.2007.11916.x

Published in:
Monthly Notices of the Royal Astronomical Society

Document Version:
Publisher's PDF, also known as Version of record

Mon. Not. R. Astron. Soc. **378,** 1619–1632 (2007) doi:10.1111/j.1365-2966.2007.11916.x

Iron abundances of B-type post-asymptotic giant branch stars in globular clusters: Barnard 29 in M 13 and ROA 5701 in ω Cen*

H. M. A. Thompson,[1]† F. P. Keenan,[1] P. L. Dufton,[1] R. S. I. Ryans,[1] J. V. Smoker,[1] D. L. Lambert[2] and A. A. Zijlstra[3]

[1]*Astrophysics Research Centre, School of Mathematics and Physics, Queen's University, Belfast BT7 1NN*
[2]*University of Texas at Austin, Austin, TX 78712–1083, USA*
[3]*School of Physics and Astronomy, University of Manchester, PO Box 88, Manchester M60 1QD*

Accepted 2007 April 24. Received 2007 April 23; in original form 2007 February 27

ABSTRACT

High-resolution optical and ultraviolet (UV) spectra of two B-type post-asymptotic giant branch (post-AGB) stars in globular clusters, Barnard 29 in M 13 and ROA 5701 in ω Cen, have been analysed using model atmosphere techniques. The optical spectra have been obtained with FEROS on the ESO 2.2-m telescope and the 2d-Coudé spectrograph on the 2.7-m McDonald telescope, while the UV observations are from the Goddard high-resolution spectrograph on the *Hubble Space Telescope* (*HST*). Abundances of light elements (C, N, O, Mg, Al and S) plus Fe have been determined from the optical spectra, while the UV data provide additional Fe abundance estimates from Fe III absorption lines in the 1875–1900 Å wavelength region. A general metal underabundance relative to young B-type stars is found for both Barnard 29 and ROA 5701. These results are consistent with the metallicities of the respective clusters, as well as with previous studies of the objects. The derived abundance patterns suggest that the stars have not undergone a gas–dust separation, contrary to previous suggestions, although they may have evolved from the AGB before the onset of the third dredge-up. However, the Fe abundances derived from the *HST* spectra are lower than those expected from the metallicities of the respective clusters, by 0.5 dex for Barnard 29 and 0.8 dex for ROA 5701. A similar systematic underabundance is also found for other B-type stars in environments of known metallicity, such as the Magellanic Clouds. These results indicate that the Fe III UV lines may yield abundance values which are systematically too low by typically 0.6 dex and hence such estimates should be treated with caution.

Key words: stars: abundances – stars: AGB and post-AGB – stars: early-type – stars: individual: NGC 6205 222 – stars: individual: NGC 5139 5701 – ultraviolet: stars.

1 INTRODUCTION

Post-asymptotic giant branch (post-AGB) stars are short-lived objects (typically 10^4 yr), of initial mass between 0.8 and 8 $M_\odot$. They have evolved from the AGB, undergone severe mass-loss, and will become planetary nebulae (Iben & Renzini 1983). This evolutionary stage has been reviewed by, for example, Kwok (1993) and Van Winckel (2003), and is important as it provides an insight into the nucleosynthesis and mixing processes during the later stages of stellar evolution. Most post-AGB stars have been identified via their infrared excess, arising from a circumstellar dust shell. This shell is most readily detected at the earliest stages of post-AGB evolution, when it is relatively hot and close to the star. As a result, the majority of post-AGBs found to date have just left the AGB, and are of A, F or G spectral type (Oudmaijer 1996).

A number of abundance studies have been performed for post-AGB stars, with the majority being metal-poor (Van Winckel 2003). However, there are many features of post-AGB evolution which are not yet fully understood. For example, several stars show abundance patterns reminiscent of interstellar gas, with Si, Ca, etc. following the very low Fe abundance, while CNO and S are near solar (Van Winckel, Waelkens & Waters 1995). Waters, Trams & Waelkens (1992) proposed a mechanism for the formation of such a 'cleaned-up' photosphere in a post-AGB star, where grain formation occurs

*This paper includes data taken at the McDonald Observatory of the University of Texas at Austin, and on the ESO 2.2-m La Silla, programme 0077.D-025(A).

†E-mail: h.thompson@qub.ac.uk

in the circumstellar shell produced in the AGB phase of the star, and subsequent slow accretion of the gas from this material results in the peculiar abundance pattern. This is most likely to happen during mass transfer between the components of a binary system, or accretion triggered by a binary companion. Indeed, Van Winckel et al. (1995) showed that all the extremely Fe-deficient post-AGB stars known at that time are binaries, providing support for this hypothesis.

Although most of the known post-AGBs are cool objects, several B-type stars originally classified as being Population I are now believed to be hot post-AGBs, on the basis of their derived atmospheric parameters and chemical compositions (see e.g. Ryans et al. 2003, and references therein). However, although the B-type stars should be evolving from the cooler post-AGBs, there are significant differences. The most striking is the large C underabundance found for several hot objects, which may imply that these left the AGB before the third dredge-up (Ryans et al. 2003).

These apparent abundance differences between the hot and cool post-AGB candidates indicate that further investigations are required, so that this evolutionary stage may be more fully understood. As a first step, it is clearly important to study hot post-AGB objects of known initial metallicity, rather than field stars of unknown origin. Fortunately, a sample of these is available: the well-known UV-Bright stars found in some globular clusters, whose post-AGB nature has been unambiguously established from their position in the cluster colour–magnitude diagram (Landsman et al. 2000).

A review of UV-Bright stars in globular clusters can be found in Moehler (2001), while searches for globular cluster post-AGB stars include Zinn, Newell & Gibson (1972), Harris, Nemec & Hesser (1983) and de Boer (1985). Of the B-type post-AGB stars studied to date, only three have well-determined iron abundance estimates, namely ZNG-1 in M 10 (Mooney et al. 2004), Barnard 29 in M 13 (Dixon & Hurwitz 1998; Moehler et al. 1998) and ROA 5701 in ω Cen (Moehler et al. 1998). Mooney et al. (2004) examined optical spectra of ZNG-1, finding an iron abundance larger than the metallicity of the cluster, M 10. Barnard 29 and ROA 5701 have been studied several times, primarily due to their relative brightness, using both optical and ultraviolet (UV) spectra (see e.g. Auer & Norris 1974; Norris 1974; Cacciari et al. 1984; de Boer 1985; Adelman et al. 1994; Conlon, Dufton & Keenan 1994; Dixon & Hurwitz 1998; Moehler et al. 1998; Thompson et al. 2006). However, the iron abundances have previously been estimated using only the UV spectra. In particular, Moehler et al. (1998) have analysed *Hubble Space Telescope* (*HST*) observations of these stars and derived Fe abundances which are lower than the cluster metallicities, which they explained by the grain-formation process discussed above. If Barnard 29 and ROA 5701 have such 'cleaned-up' photospheres, then one would expect them to show similar depletions in Mg and Si, which are also subject to grain formation. However, previous studies of Barnard 29 and ROA 5701 indicate no depletions in Mg or Si (Conlon et al. 1994; Moehler et al. 1998; Thompson et al. 2006).

Clearly, the abundances of Barnard 29 and ROA 5701 need revisiting, in particular those for Fe. In this paper, high-resolution optical and UV spectra of Barnard 29 and ROA 5701 are analysed, using model atmosphere techniques to estimate atmospheric parameters and chemical compositions. The observations and data reduction are discussed in Section 2, while Section 3 details the analysis methods and results. In Section 4 we present a discussion of our results, and in particular we assess the accuracy of Fe abundance determinations for B-type stars using UV spectra.

2 OBSERVATIONS AND DATA REDUCTION

Optical spectra of Barnard 29 and ROA 5701 were obtained during two observing runs, the former with the 2.7-m Harlan J. Smith Telescope (McDonald Observatory) on three nights between 2005 April 30 and May 5, and the latter with the MPG/ESO 2.2-m Telescope (La Silla, Chile) on 2006 April 10. UV spectra of both stars were taken from the *HST* archive. Details of the observations are provided below.

2.1 Optical spectra

2.1.1 Barnard 29

Barnard 29 was observed with the 2d-Coudé spectrograph (Tull et al. 1995), using a 2.4-arcsec slit to achieve a spectral resolution ($R = \lambda/\Delta\lambda$) of ∼35 000 and a wavelength coverage of ∼3700–10 000 Å. Due to cloud, data were taken only on three nights, resulting in 30 half-hour exposures, or 15 h on-source. A Th–Ar hollow cathode lamp was observed at the beginning and end of each night, with the centres of the lines stable to better than ∼0.1 pixel. Test exposures were taken at the start of the run, to ensure that optical ghosts ('the picket fence'; Cheng & Chang 2000) and bad columns did not overlap with wavelength regions of interest, in particular the Fe III lines around 4420 Å. Also, in order to ensure that the weak absorption-line features detected were real, the central wavelength was changed by ∼0.4 Å, after the first night and remained in the new position for the other two clear nights.

The data were reduced using standard methods within the Image Reduction and Analysis Facility (IRAF; Barnes 1993). This reduction included bias subtraction and flat-fielding, with stellar extraction and cosmic ray removal performed using DOECSLIT (Valdes 1993) and SCOMBINE. The signal-to-noise ratio (S/N) per pixel in the co-added spectrum was ∼130 per pixel at ∼4420 Å (corresponding to ∼180 per resolution element), and this was read into the Starlink package DIPSO (Howarth et al. 2004) for further analysis (see Section 2.1.3).

2.1.2 ROA 5701

The optical spectra of ROA 5701 were obtained using the high-resolution Fibre-fed Extended Range Optical Spectrograph (FEROS; Kaufer et al. 1999), with the EV 2000 × 4000 CCD detector and a 79 lines mm^{-1} échelle grating. In total, ROA 5701 was observed for 9 h, resulting in a spectral resolution of $R \sim 46\,000$ and a wavelength coverage of ∼3560–9200 Å.

The data were reduced online, using the standard FEROS Data Reduction System, implemented with ESO–MIDAS software. This reduction includes the extraction and deblazing of the échelle orders, wavelength calibration and merging of the orders. The reduced spectral exposures were combined into a single spectrum using SCOMBINE within IRAF, and this was imported into DIPSO for further analysis (see Section 2.1.3). An average S/N of ∼85 per pixel at ∼4420 Å was obtained, corresponding to ∼120 per resolution element.

2.1.3 Equivalent width measurements

Initially, the continua of the optical spectra for both Barnard 29 and ROA 5701 were normalized using low-order polynomials fitted to spectral regions free from absorption features. The line-fitting program ELF within DIPSO was then employed to measure absorption-line equivalent widths, by fitting Gaussian profiles to the lines (see Thompson et al. 2006, for further details). Balmer lines and diffuse

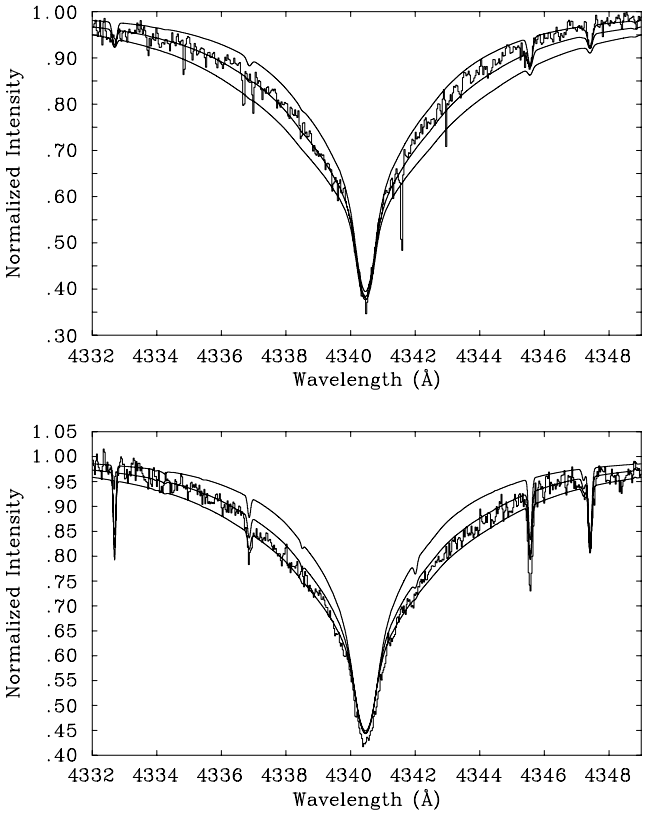

Figure 1. Observed and theoretical line profiles for Hγ at 4341 Å in the spectra of Barnard 29 (upper panel) and ROA 5701 (lower panel). The theoretical profiles have been generated for surface gravities of 2.75, 3.0 and 3.25 dex (upper, middle and lower smooth curves, respectively) for Barnard 29, implying a surface gravity of 2.95 dex. For ROA 5701, results have been calculated for surface gravities of 3.0, 3.25 and 3.5 dex (upper, middle and lower smooth curves, respectively), implying log $g = 3.3$ dex.

He I line equivalent widths were not measured, as instead theoretical profiles were fitted to the normalized data (see e.g. Fig. 1).

2.2 UV spectra

The UV spectra of Barnard 29 and ROA 5701 were obtained directly from the *HST* Multimission Archive (http://archive.stsci.edu; z3EC0204T and z3EC0104M, respectively). They were observed with the Goddard high-resolution spectrograph (GHRS) using the G200M grating ($R = 25\,000$) and the large science aperture (LSR), giving a wavelength coverage of ∼1860–1906 Å. Focal-plane (FP) splits were not used for these observations (Moehler et al. 1998). Barnard 29 was observed on 1996 November 30 for 4570 s, and ROA 5701 on 1996 August 3 for 4711 s.

Following the standard pipeline reduction, the spectra were co-aligned within IRAF, using the STSDAS package (Version 3.4). The combined spectrum for each star was then read into DIPSO and cross-correlated with theoretical spectra to obtain the stellar LSR radial velocities of −228 and +258 km s^{-1} for Barnard 29 and ROA 5701, respectively. These are consistent with the radial velocities of M 13 (−227.2 km s^{-1}, Harris 1996) and ω Cen (+240 km s^{-1}, Norris 1974). An interstellar reddening correction, of $E(B - V) = 0.02$ (Harris 1996) for M 13 and $E(B - V) = 0.11$ (Cacciari et al. 1984) for ω Cen, was applied to the appropriate spectrum. The spectra were then binned, with a wavelength interval of 0.05 Å, resulting in a wavelength coverage of 1868–1906 Å for Barnard 29 and 1865–1903 Å for ROA 5701.

3 DATA ANALYSIS AND RESULTS

3.1 Model atmosphere calculations

Non-local thermodynamic equilibrium (non-LTE) model atmosphere grids, calculated using TLUSTY and SYNSPEC (Hubeny 1988; Hubeny & Lanz 1995; Hubeny, Heap & Lanz 1998), have been used to derive atmospheric parameters and chemical abundances. A summary of the procedures involved are given in Thompson et al. (2006), while a more detailed discussion of the grids and methods may be found in Ryans et al. (2003) and Dufton et al. (2005), and also at http://star.pst.qub.ac.uk.

Briefly, four grids have been produced with metallicities corresponding to [Fe/H] = 7.5 dex for the Galaxy, 7.2 and 6.8 dex for the Large (LMC) and Small (SMC) Magellanic Clouds, respectively, and 6.4 dex for low-metallicity regimes. For each metallicity grid, approximately 3000 models were calculated for a range of effective temperatures from 12 000 to 35 000 K, logarithmic gravities (log $g =$ 4.5 dex down to the Eddington limit) and microturbulences of 0 to 30 km s^{-1}. The iron abundance was fixed at each grid, while the light element abundances (C, N, O, Mg, Si, S) were allowed to vary from −0.8 to +0.8 dex around their base (metallicity) value. Iron is assumed to dominate the metal line blanketing. However, the exclusion of nickel in our models should not be a significant source of error in the atmospheric parameters and chemical composition (Hubeny et al. 1998). The atmospheric structure is therefore defined by the iron abundance (metallicity), effective temperature, gravity and microturbulence. It is also assumed that light element abundances can vary with negligible effect on the atmospheric structure, as shown in tests performed by Dufton et al. (2005).

Theoretical profiles and equivalent widths of light element transitions were calculated using the models. A GUI interface in IDL allows the user to access the theoretical equivalent widths and interpolate these to calculate equivalent widths and abundance estimates for ∼200 metal lines, for any set of atmospheric parameters. Abundance increments of 0.4 dex used in the grids were found to be sufficiently small that no significant errors were incurred due to the interpolation procedures (Ryans et al. 2003).

3.2 Atmospheric parameters

The atmospheric parameters of each star were determined from the optical spectra. As the parameters are interrelated, an iterative process is used (see e.g. Kilian 1992; Hunter et al. 2005; Thompson et al. 2006). Studies of giants in M 13 yield a cluster metallicity of [Fe/H] = −1.6 (Yong, Aoki & Lambert 2006), while for ω Cen, which contains at least three stellar populations, the main cluster giant population indicates [Fe/H] = −1.6 (Origlia et al. 2003). Hence, for both stars the grid corresponding to low-metallicity regions (6.4 dex; −1.1 dex lower than Galactic) was used, as this was the lowest metallicity model available and thus the most appropriate based on the metallicities of the respective clusters. Lee et al. (2005) found that using grids of different iron abundances changed the effective temperature estimate by typically $\leqslant$500 K, while the gravity and microturbulence estimates were unaffected, so the use of this grid should not be a major source of error. The adopted atmospheric parameters and associated errors for both stars are listed in Table 1.

Table 1. Adopted atmospheric parameters for Barnard 29 and ROA 5701.

Star	$T_{\rm eff}$ (10^3 K)	log g (dex)	ξ (km s^{-1})	$\upsilon \sin i$ (km s^{-1})
Barnard 29	20 ± 1	2.95 ± 0.1	4 ± 2	0
ROA 5701	25 ± 1	3.3 ± 0.1	1^{+2}_{-1}	3

Effective temperature estimates, $T_{\rm eff}$, were determined using the silicon ionization balance, with Si II/Si III employed for Barnard 29 and Si III/Si IV for ROA 5701. Surface gravities, log g, were derived by overplotting the observed spectrum in the regions of the Balmer lines with theoretical profiles, with associated errors assessed from the uncertainty in the fitting (Fig. 1). The microturbulence, ξ, was determined using the observed O II and Si III lines, by removing the dependence of abundance on line strength, that is, a plot of abundance against line strength having a zero gradient (Kilian 1992). Individual multiplets were employed in this procedure, to reduce errors which may arise from using many different multiplets (Hunter et al. 2005).

Initial atmospheric parameters for Barnard 29 were taken from Conlon et al. (1994), and are $T_{\rm eff} = 20\,000$ K, log$g = 3.0$ and $\xi = 10$ km s^{-1}. The temperature estimate remained unchanged at 20 000 K with an associated error of $\pm$1000 K, the gravity was constrained to log $g = 2.95 \pm 0.10$, while a determination of the microturbulence led to a value of $\xi = 4 \pm 2$ km s^{-1}.

For ROA 5701, initial parameters were taken from Thompson et al. (2006), namely $T_{\rm eff} = 25\,000$ K, log $g = 3.25$ and $\xi = 5$ km s^{-1}. The present analysis led to no change in the effective temperature. As no absorption line was detected for He II 4541 Å, assuming a normal helium abundance also allowed us to place an independent upper limit of $T_{\rm eff} < 26\,000$ K. Therefore, the associated error for $T_{\rm eff}$ is $\pm$1000 K. The gravity was determined to be log $g = 3.3 \pm 0.1$, and the microturbulence $\xi = 1^{+2}_{-1}$ km s^{-1}.

3.2.1 Rotational velocity, $\upsilon \sin i$

In addition to the microturbulent broadening, some rotational broadening may occur. The effect of this was investigated by fitting instrumentally broadened non-LTE theoretical profiles for the Si III multiplet at 4560 Å, calculated using the appropriate $T_{\rm eff}$, log g and ξ values, to the observed spectra. The theoretical profiles were rotationally broadened and overlain in order to determine the most appropriate $\upsilon \sin i$ (see Trundle et al. 2001 for further details). For Barnard 29, the profile fitting resulted in a value of $\upsilon \sin i = 0$ km s^{-1}, while in the case of ROA 5701, a $\upsilon \sin i = 3$ km s^{-1} was obtained.

Lehner et al. (2000) discuss the difficulty in differentiating between the effects of the two types of broadening when such low values are obtained. In order to place an upper limit on the $\upsilon \sin i$ values, a microturbulence of 0 km s^{-1} was assumed for both stars, as a non-zero microturbulence would lead to lower $\upsilon \sin i$ estimates (Trundle et al. 2001). This resulted in, for Barnard 29 $\upsilon \sin i \leqslant 6$ km s^{-1} and for ROA 5701, $\upsilon \sin i \leqslant 3$ km s^{-1}.

3.3 Abundances from optical spectra

Abundances for both stars were determined using the adopted atmospheric parameters; atomic data were taken from http://star.pst.qub.ac.uk. Table 2 contains the equivalent width measurements for the observed metal lines, along with the associated abundance estimates. If more than one line contributed to an equivalent width, the lines were treated as blends within TLUSTY.

There are currently no non-LTE grids available for Al III, S III or Fe III, although sulphur is included in our non-LTE model atmosphere calculations using a relatively simple model. Using TLUSTY, models were calculated, adopting the appropriate atmospheric parameters. These were then employed to generate theoretical LTE equivalent widths (see Hunter et al. 2005), which were used to derive the abundance estimates shown in Table 2, with errors calculated by utilizing the same method as for other elements.

Table 3 contains a summary of the abundances for each species, along with the associated error estimates and the number of lines observed. Also included are the abundances previously derived for the objects (Conlon et al. 1994; Dixon & Hurwitz 1998; Moehler et al. 1998; Thompson et al. 2006), and those of normal B-type stars, both in the Galactic cluster NGC 6611 (Hunter et al. 2007) and in the local field (Kilian 1992, 1994). The former were determined using the same TLUSTY code as employed in the present paper. Also included are typical interstellar medium (ISM) abundances for the elements concerned, as listed in Wilms, Allen & McCray (2000). The C, N and O abundances are taken from Cardelli et al. (1996) and Meyer, Cardelli & Sofia (1997); Meyer, Jura & Cardelli (1998), respectively, with all other elements given by Snow & Witt (1996). The Al abundance, however, is taken as 70 per cent of the adopted solar abundance of Wilms et al. (2000), as ISM abundances appear to be reduced by 20–30 per cent with respect to solar abundances (Savage & Sembach 1996; Snow & Witt 1996).

The errors associated with the absolute abundances (see Table 3) arise from systematic and random errors (full details can be found in Hunter et al. 2005). Random errors are connected with the data analysis, for example: line-fitting errors, oscillator strengths and observational uncertainties. The random uncertainty is taken as the s.d. in the abundances of a given species, divided by the square root of the number of lines observed for that species. Where only one line was detected, the s.d. is that of the best observed species, for example, O II. Systematic errors arise from the uncertainties in the atmospheric parameters, and are estimated by varying each parameter by its associated errors. The total uncertainty is the square root of the sum of the squares of the random and systematic errors. We note that the scatter of individual abundances for each species is reasonably small, with any discrepancies probably arising from poorly determined lines and possible errors in atomic data.

A normal He abundance has been assumed throughout the analysis of both stars, which was tested by overplotting theoretical spectra on the observations in regions containing He I absorption features. There is good agreement to within the uncertainties of the atmospheric parameters, suggesting this is a valid assumption. When lines are badly blended with hydrogen or helium lines, they are not included in the non-LTE calculations.

For both stars, the best observed species are N II and O II, with the majority of equivalent widths believed to be accurate to better than 20 per cent. If the lines of poorer quality are removed, the abundance estimates remain unchanged (within the error bars), indicating that data of poorer quality do not significantly affect the abundances obtained.

The C abundances for both Barnard 29 and ROA 5701 in Table 3 are quoted as upper limits. Due to the quality of the spectra, it was only possible to place upper limits on the equivalent widths of the C II lines at 4267 and 6578 Å. Sigut (1996) finds that the 4267 Å multiplet gives a limiting precision of $\sim \pm 0.2$ dex, over a $T_{\rm eff}$ range of 15 000–31 000 K (as reproduced by Nieva & Przybilla 2006). However, for $T_{\rm eff} < 25\,000$ K, the line at 6578 Å is somewhat more

Table 2. Absorption-line equivalent width measurements from optical spectra and derived abundances for Barnard 29 and ROA 5701.

Identification		Barnard 29				ROA 5701			
Rest λ (Å)	Species	Observed λ (Å)	W (mÅ)	Quality[†]	Abundance[◇]	Observed λ (Å)	W (mÅ)	Quality[†]	Abundance[◇]
4267.00	C II[a]	–	<10	–	<6.13	–	<10	–	<6.27
6578.05	C II	–	<10	–	<6.64	–	<10	–	<6.54
3995.00	N II[a]	3995.00	65	a	7.22	3995.00	45	a	6.99
4035.08	N II	4035.09	12	c	7.62	–	–	–	–
4041.31	N II	4041.32	25	a	8.30	–	–	–	–
4043.53	N II	4043.52	14	b	7.47	–	–	–	–
4227.74	N II	4227.71	8	c	7.36	–	–	–	–
4241.78	N II[a]	4241.79	21	a	7.62	4241.82	15	c	7.67
4432.73	N II[a]	4432.72	12	c	7.39	4432.75	11	c	7.35
4447.03	N II	4446.99	30	a	7.28	4447.03	18	b	6.95
4601.48	N II	4601.47	27	a	7.34	–	–	–	–
4607.16	N II	4607.14	21	b	7.29	–	–	–	–
4613.86	N II	4613.85	18	a	7.34	–	–	–	–
4621.29	N II	4621.38	16	a	7.12	–	–	–	–
4630.54	N II	4630.56	50	a	7.28	4630.55	26	b	6.93
4643.09	N II	4643.10	27	a	7.33	4643.10	11	c	6.93
5001.10	N II[a,b]	5001.12	30	b	7.36	5001.16	20	a	6.92
5001.50	N II[a,b]	5001.47	37	b	–	5001.50	25	a	–
5002.70	N II[a,b]	5002.68	8	c	–	–	–	–	–
5005.15	N II	5005.15	47	b	7.34	5005.17	30	a	6.88
5007.33	N II	5007.23	30	c	7.68	5007.34	11	b	6.96
3911.96	O II[a,b]	–	–	–	–	3911.98	27	a	7.64
3912.09	O II[a,b]	–	–	–	–	–	–	–	–
3919.28	O II	–	–	–	–	3919.30	19	b	7.74
3945.04	O II	–	–	–	–	3945.04	15	b	7.62
3954.37	O II	–	–	–	–	3954.38	29	a	7.65
3982.72	O II	–	–	–	–	3982.72	20	b	7.78
4069.62	O II[a,b]	4069.61	13	b	7.55	4069.64	36	a	7.76
4069.89	O II[a,b]	4069.87	17	b	–	4069.90	47	a	–
4072.16	O II	4072.13	23	a	7.52	4072.17	57	a	7.72
4075.86	O II	4075.83	30	a	7.54	4075.87	68	a	7.71
4078.84	O II	–	–	–	–	4078.85	19	b	7.79
4089.29	O II	–	–	–	–	4089.29	33	a	8.02
4132.80	O II	–	–	–	–	4132.81	24	b	7.76
4185.46	O II	–	–	–	–	4185.47	24	a	7.67
4294.79	O II	–	–	–	–	4294.77	11	c	7.56
4303.84	O II[a]	–	–	–	–	4303.85	15	c	7.39
4317.14	O II[a]	4317.12	10	a	7.35	4317.15	37	a	7.78
4319.63	O II	4319.61	13	a	7.52	4319.64	46	a	7.95
4349.43	O II	4349.43	25	a	7.59	4349.43	71	a	7.96
4351.26	O II[a]	4351.25	9	c	7.29	4351.27	38	a	7.54
4366.90	O II[a]	4366.86	12	b	7.40	4366.90	37	a	7.72
4369.27	O II	–	–	–	–	4369.30	10	c	7.80
4395.94	O II	–	–	–	–	4395.95	11	c	7.69
4414.91	O II	4414.90	26	a	7.53	4414.91	70	a	7.86
4416.98	O II	4416.98	20	a	7.64	4416.98	52	a	7.89
4452.38	O II	–	–	–	–	4452.37	16	b	7.90
4590.97	O II	4590.98	11	b	7.41	4590.99	43	a	7.66
4596.17	O II	4596.17	8	c	7.38	4596.19	33	a	7.61
4609.44	O II[a]	–	–	–	–	4609.44	12	c	7.36
4638.86	O II	4638.87	14	a	7.54	4638.87	50	a	7.87
4641.81	O II	4641.83	27	a	7.52	4641.83	79	a	7.85
4649.14	O II[a,b]	4649.14	39	a	7.53	4649.16	102	a	7.86
4650.84	O II[a,b]	4650.84	14	a	–	4650.86	48	a	–
4661.64	O II	4661.63	18	a	7.61	4661.65	50	a	7.81
4673.74	O II	–	–	–	–	4673.75	13	b	7.90
4676.24	O II	4676.21	16	b	7.62	4676.25	44	a	7.83
4699.00	O II[a,b]	–	–	–	–	4699.03	34	c	7.63
4699.22	O II[a,b]	–	–	–	–	4699.24	–	b	–
4705.35	O II	–	–	–	–	4705.37	37	a	7.70
4710.01	O II[a]	–	–	–	–	4710.04	11	c	7.93

Table 2 – *continued*

Identification		Barnard 29				ROA 5701			
Rest λ (Å)	Species	Observed λ (Å)	W (mÅ)	Quality†	Abundance◇	Observed λ (Å)	W (mÅ)	Quality†	Abundance◇
4890.93	O II	–	–	–	–	4890.87	11	a	7.79
4906.83	O II	–	–	–	–	4906.84	15	c	7.60
4924.53	O II	–	–	–	–	4924.53	28	a	7.91
4941.07	O II	–	–	–	–	4941.10	12	c	7.90
4943.00	O II[a]	–	–	–	–	4943.01	21	a	7.94
4481.13	Mg II[a,b]	4481.12	19	a	6.10	4481.16	10	b	6.15
4481.33	Mg II[a,b]	4481.32	11	b	–	4481.34	7	b	–
4128.05	Si II	4128.04	11	c	6.45	–	–	–	–
4552.62	Si III	4552.60	71	a	6.45	4552.63	67	a	6.18
4567.82	Si III	4567.86	53	a	6.43	4567.86	50	a	6.18
4574.76	Si III	4574.77	30	a	6.48	4574.77	23	a	6.16
5739.74	Si III	5739.76	26	b	6.59	5739.78	23	b	5.96
4088.85	Si IV	–	–	–	–	4088.89	33	a	6.15
4116.10	Si IV	–	–	–	–	4116.12	21	b	6.17
4512.54	Al III	4512.58	7	b	5.13	–	–	–	–
4529.18	Al III	4529.18	11	b	5.15	–	<5	–	<4.87
4253.59	S III	4253.57	7	a	5.72	4253.60	14	b	5.62
4419.60	Fe III	4419.60	3	c	6.03	–	–	–	–
5156.12	Fe III	5156.09	5	c	6.08	–	–	–	–
5833.93	Fe III	5833.94	4	c	6.21	5833.99	<6	c	<6.10

† 'a' indicates that the equivalent width measurement should be accurate to better than ±10 per cent, 'b' to better than ±20 per cent and 'c' to less than ±20 per cent. ◇Logarithmic abundance [M/H] on the scale log[H] = 12.00. [a]Treated as blends in TLUSTY. [b]Equivalent widths of adjacent lines were combined to produce the corresponding abundances shown.

Table 3. Absolute abundances for Barnard 29 and ROA 5701 from their optical spectra, along with those previously derived by Conlon et al. (1994); Dixon & Hurwitz (1998); Moehler et al. (1998) and Thompson et al. (2006). Also listed are abundances for normal B-type stars from the local field (Kilian 1992, 1994) and the Galactic cluster NGC 6611 (Hunter et al. 2007), plus values for the interstellar medium (Cardelli et al. 1996; Snow & Witt 1996; Meyer et al. 1997, 1998; Wilms et al. 2000). Bracketed values are the number of lines of each species observed.

Species	Barnard 29					ROA 5701				B-type		ISM
	This paper		Con 94	Dix 98	Moe 98*	This paper		Moe 98[a]	Tho 06	Kil 92/94	Hun 06	
C II	<6.64	(1)	<6.70	6.15	–	<6.54	(1)	<5.85	<6.51	8.20	7.95	8.38
N II	7.43 ± 0.12	(17)	7.30	–	–	7.06 ± 0.12	(9)	6.86	7.05	7.69	7.59	7.88
O II	7.50 ± 0.24	(17)	7.60	–	–	7.76 ± 0.10	(41)	7.97	7.75	8.55	8.55	8.69
Mg II	6.10 ± 0.15	(1)	6.00	–	–	6.15 ± 0.21	(1)	–	6.27	7.38	7.32	7.40
Si II	6.45 ± 0.20	(1)	–	–	–	–		–	–	–	–	–
Si III	6.45 ± 0.26	(3)	6.30	–	–	6.17 ± 0.20	(3)	6.14	5.94	7.28	7.41	7.27
Si IV	–		–	–	–	6.16 ± 0.40	(2)	–	5.95	–	–	–
Al III	5.14 ± 0.10	(2)	5.19	–	–	<4.87	(1)	–	<5.21	6.22	–	6.33
S III	5.72 ± 0.26	(1)	<6.29	5.34	–	5.62 ± 0.23	(1)	–	5.71	7.25	–	7.09
Fe III	6.07 ± 0.12	(3)	<6.70	5.28	5.30	<6.10	(1)	4.79	–	–	7.50	7.43

[a]Average of curve-of-growth and spectrum synthesis values.

reliable than that at 4267 Å. Therefore, the upper limits given in Table 3 are based on the 6578 Å line alone.

The Mg II doublet at 4481 Å was observed and treated as a blend within TLUSTY, and for both stars the derived abundances appear reliable. We note that the Si abundance estimates are sensitive to the adopted atmospheric parameters. For example, for Barnard 29 a change in $T_{\rm eff}$ of ±1000 K leads to a variation of ±0.15 dex in the abundance of Si II and ±0.21 for Si III. In the case of ROA 5701, the same temperature change produces an abundance variation of ±0.10 dex for Si III and ±0.34 dex for Si IV.

The Si III line at 5739 Å was observed in both stars. However, as there are no non-LTE grids available for this spectral region, theoretical LTE equivalent widths were generated, as for S III, Al III and Fe III. The resulting LTE abundances are 6.59 dex for Barnard 29 and 5.96 dex for ROA 5701, which compare well to the Si III results in Table 3. Gies & Lambert (1992) and Kilian (1994) found that LTE abundances agree to 0.2 dex with corresponding non-LTE abundances for B-type stars, consistent with the results here. However, as the 5739 Å abundances are in LTE, they are not included in the relevant non-LTE Si III results listed in Table 3.

The S III 4254 Å line was used to derive the S abundance in both Barnard 29 and ROA 5701. As previously noted, these abundances are based on theoretical LTE S III equivalent widths. Hunter et al. (2005) find that non-LTE effects appear to be negligible for

this species. Additionally, we have carried out test calculations and find little difference between the S III spectrum predicted using LTE or non-LTE. Hence our use of an LTE approach is probably valid.

Two Al III lines, at 4512 and 4259 Å, were observed for Barnard 29. No Al features were detected for ROA 5701, but an upper limit on the Al abundance was set using the 4529 Å line. The Al abundances are treated in LTE, but should be reliable as Hunter et al. (2005) state that when using the dominant ion stage, LTE abundance calculation will give good agreement with non-LTE abundances.

Three Fe III lines were observed at 4419, 5156 and 5833 Å in Barnard 29, with one in ROA 5701 at 5833 Å. The S/N of the local continuum for the lines are ∼130, 155, 150 and 110 per pixel, respectively. LTE calculations were used to determine the Fe abundance, and Fig. 2 shows theoretical profiles corresponding to the measured abundances, overplotted on to the observed spectra of Barnard 29 (a, b and c) and ROA 5701 (d). As can be seen from the figure, some of the features are difficult to distinguish from the noise. Indeed, Fig. 2(a) appears to show the 4419 Å line in Barnard 29, but numerous noise features of similar size to the 4419 Å line can also be seen, which may be due to observational effects or the reduction process. Unless these additional features are real (which is unlikely), then the Fe III line may also not be real and hence the abundance derived should be used with care. In addition, the 4419 Å line appears to be narrower than other weak stellar absorption features in the spectrum, as may be seen from the profile fit in Fig. 2(a), where the theoretical feature is wider than that observed. However, 4419 Å gives a similar abundance to the apparently more reliable 5156 Å line, and so all three observed Fe III transitions are used in determining the iron abundance for Barnard 29. Also, these lines have the largest *gf*-values in their respective multiplets, and are among the strongest unblended Fe III lines in the optical spectral region. For ROA 5701, the sole Fe III line observed at 5833 Å does not appear reliable (see Fig. 2d) and hence the abundance is taken as an upper limit.

As the observed optical iron lines are of low-quality, UV spectra were also employed to determine Fe abundances for both Barnard 29 and ROA 5701. This is discussed below.

3.4 Iron abundances from UV spectra

To determine an iron abundance from the GHRS/*HST* spectrum, a goodness-of-fit method was used (Ryans et al. 2002; Dufton et al. 2006, Dufton (in preparation)). Theoretical spectra were generated for the regions observed by the GHRS/*HST*, using non-LTE TLUSTY model atmospheres and appropriate stellar atmospheric parameters. The model grid for low-metallicity regions was again used, and the underabundance of elements (heavier than He, up to and including Zn), was varied in each spectrum (in steps of 0.1 dex from 0.0 to −2.5 dex) relative to the solar estimates adopted in TLUSTY (Grevesse & Sauval 1998). Light elements (C, N, O, Mg, Si) were treated in non-LTE while all other elements were in LTE. Dufton (in preparation) found that ∼80 per cent of absorption in the UV spectral region covered by our GHRS/*HST* data are due to Fe, with more than 95 per cent from Fe-group elements, therefore the calculations are taken as being in LTE. Iron dominates the absorption; therefore any variation in the relative element abundances should not significantly affect the theoretical spectra.

Due to the numerous absorption features in the UV spectral region, continuum placement was difficult, as may be seen from the GHRS/*HST* observations of Barnard 29 and ROA 5701 in Fig. 3. Therefore, the continuum was not normalized; instead the flux calibrated spectrum was examined. This was achieved by smoothing the theoretical spectra with a Gaussian function (to allow for instrumental broadening), followed by binning to the exact wavelength range and interval as the observed spectra, and then scaling to the same mean flux as that observed.

A goodness-of-fit was calculated by finding the sum of the squares of the difference between the observed and theoretical spectra for a range of metallicities. A plot of this produced a parabolic shape, with the model with the best goodness-of-fit situated at the

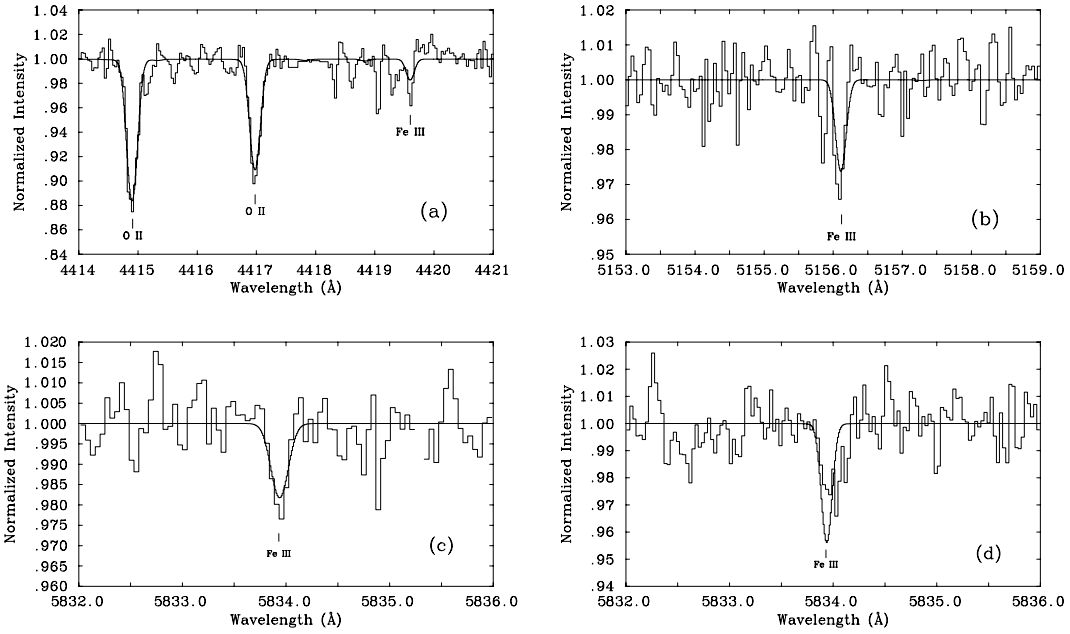

Figure 2. Observed and theoretical line profiles for Fe III in Barnard 29 (a, b and c) and ROA 5701 (d). The theoretical profiles (smooth lines) are the best fits to the observed features, and have been calculated at abundances of (a) O II 4414 Å = 7.53 dex, O II 4416 Å = 7.64 dex and Fe III 4419 Å = 6.03 dex; (b) Fe III 5156 Å = 6.08 dex; (c) Fe III 5833 Å = 6.21 dex and (d) Fe III 5833 Å = 6.10 dex.

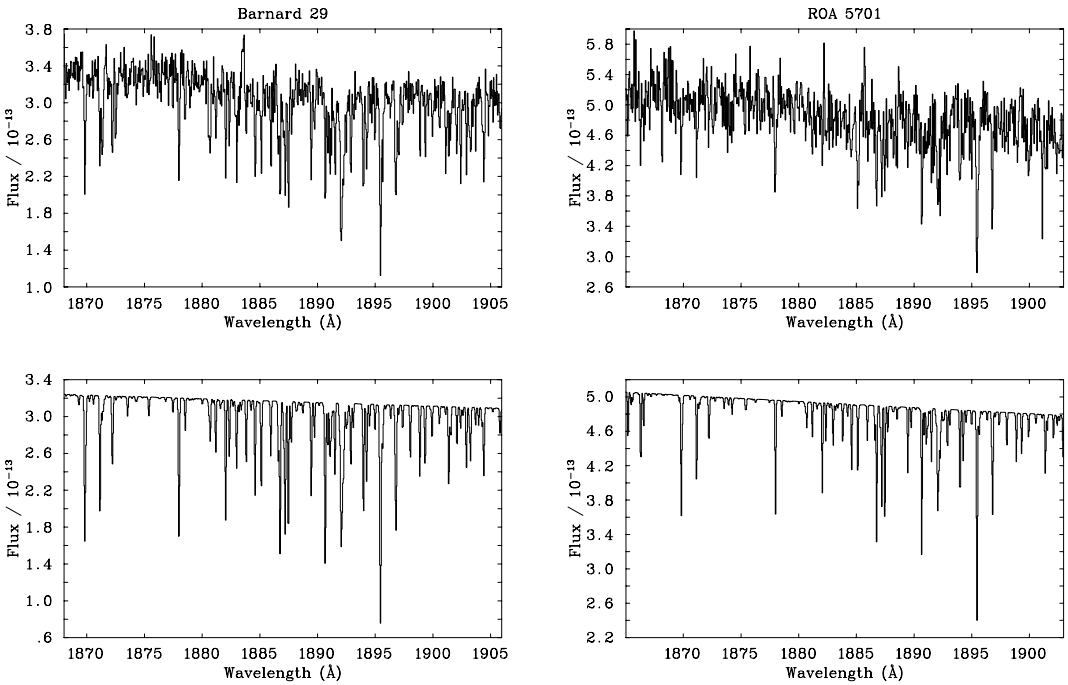

Figure 3. The upper panels show the observational data for Barnard 29 and ROA 5701 obtained with GHRS/*HST*, while the lower panels contain the theoretical spectra for [Fe/H] = −2.1 and −2.4, respectively, relative to the Galactic value of [Fe/H] = 7.5.

minimum of the parabola. This method removes the need to normalize the observed spectrum, thus reducing errors associated with fitting the continuum. To test if different spectral intervals would affect the abundance estimate, smaller wavelength ranges were selected and analysed. No significant change was found in the goodness-of-fit and associated metallicity value.

Results of the minimization procedure are shown in Table 4, along with iron abundances derived by Moehler et al. (1998) and Dixon & Hurwitz (1998). Errors were calculated using a similar method as for the optical spectra. Systematic errors were obtained by varying the atmospheric parameters by their respective errors, while random errors were estimated by overplotting theoretical spectra around the minimum and observing where the spectrum no longer matched the strongest observed features. The total uncertainty was then calculated and is shown in Table 4.

The theoretical spectra that produced a minimum are shown, together with the observed spectra, in Fig. 3. For Barnard 29, the goodness-of-fit indicates an [Fe/H] = −2.1. In general, the theoretical spectrum matched many of the individual absorption features in the observational data, supporting the abundance estimates for this star. ROA 5701 was less convincing in the fitting of the observed spectrum, with a minimum produced for [Fe/H] = −2.4 dex. In particular, the spectrum has fewer identifiable absorption features compared to Barnard 29, making the estimation of the metallicity unreliable.

Table 4. Values of [Fe/H] derived for Barnard 29 and ROA 5701 relative to the Galactic abundance, along with previous estimates.

Star	This paper	Moehler et al. (1998)	Dixon & Hurwitz (1998)
Barnard 29	-2.1 ± 0.1	−2.2	−2.2
ROA 5701	-2.4 ± 0.3	−2.7	–

In Fig. 3, there is an emission feature at ∼1883 Å in the spectrum of Barnard 29, which appears real and resembles part of a P Cygni profile. However, the apparent line does not have a strong associated absorption feature and is therefore thought to be an artefact of the reduction process. If it is removed from the goodness-of-fit analysis, there is no change in the abundance obtained. The feature was not observed in ROA 5701.

4 DISCUSSION

Barnard 29 and ROA 5701 have been the subject of numerous studies, several of which have included determinations of atmospheric parameters and chemical compositions. We discuss these below in the context of the present results.

4.1 Comparison of atmospheric parameters

4.1.1 Barnard 29

Previous studies of Barnard 29 have produced similar atmospheric parameters to those found in this paper. For example, Auer & Norris (1974) used non-LTE models with optical spectra to derive $T_{\rm eff} = 22\,500 \pm 1200$ K and $\log g = 3.0 \pm 0.15$ dex, while de Boer (1985) employed UV spectra from the *IUE* satellite and UV colours, finding $T_{\rm eff} = 19\,000 \pm 1000$ K and $\log g = 3.2$ dex. These spectra were again employed by Adelman et al. (1994), along with optical spectra of Hγ, to determine LTE atmospheric parameters of $T_{\rm eff} = 20\,250$ K and $\log g = 3.15$ dex. Conlon et al. (1994) used LTE models to analyse *IUE* low-resolution data and WHT/UES optical data, resulting in $T_{\rm eff} = 20\,000 \pm 1000$ K, $\log g = 3.0 \pm 0.1$ dex and $\xi = 10 \pm 2$ km s^{-1}. Dixon & Hurwitz (1998) took a sample of the *IUE* spectra used by Conlon et al. (1994), along with *ORFEUS-SPAS II* spectra, and with LTE techniques obtained the same surface

gravity as Conlon et al. (1994), but an increased temperature estimate of $T_{\rm eff} = 21\,000 \pm 1000$ K.

The previously derived effective temperatures and surface gravities are in good agreement with those found in this paper, within the errors, with the exception of the Auer & Norris (1974) temperature, which may be due to using different non-LTE models. Conlon et al. (1994) derived a larger microturbulence than in the present paper, presumably due to using LTE models rather than our non-LTE approach. Also Conlon et al. (1994) only employed O II lines in their determination of ξ, compared to our use of both the Si III multiplet and a variety of different multiplets of O II. Given the high quality of our observational data combined with the complexity of our non-LTE models, we believe that our atmospheric parameters for Barnard 29 are probably the most reliable estimates to date.

4.1.2 ROA 5701

ROA 5701 was studied recently by Thompson et al. (2006) using the same non-LTE models and methods as in the present paper, resulting in atmospheric parameters of $T_{\rm eff} = 25\,000 \pm 1000$ K, $\log g = 3.2 \pm 0.2$ dex and $\xi = 5 \pm 5$ km s^{-1}. Moehler et al. (1998) employed ESO CASPEC optical spectra, along with the GHRS/*HST* data used here, and found $T_{\rm eff} = 22\,000$–$24\,500$ K, $\log g = 3.2$–3.4 dex. In addition, they derived $\xi = 2$–3 or 20 km s^{-1}, the former using Fe III transitions and the latter those of O II. Their use of LTE models, compared to the non-LTE approach in the present paper, may be the reason for the differences in the derived microturbulence values. The present microturbulence estimate is smaller than that of Thompson et al. (2006), probably due to improved equivalent width measurements and surface gravity estimate, although it is still within the uncertainty quoted.

Other studies of ROA 5701 include Norris (1974), who analysed narrow-band and UBV photometry to obtain $T_{\rm eff} = 26\,600$ K and $\log g = 3.5$ dex, and Cacciari et al. (1984) who used *IUE* spectra to derive $T_{\rm eff} = 24\,000$ K. These studies are in agreement with the parameters derived here, with the exception of the $T_{\rm eff}$ estimate of Norris (1974). Cacciari et al. (1984) suggested that the different values of $(B-V)$ used by Norris (1974) are responsible for their larger temperature estimate. The results derived here are hence generally consistent with previous values, but once again are believed to be more reliable due to the improved observational data and non-LTE models employed in our analysis.

4.2 Comparison of chemical compositions

Table 3 shows the absolute abundances derived for Barnard 29 and ROA 5701, along with those previously determined by Conlon et al. (1994), Moehler et al. (1998) and Dixon & Hurwitz (1998) for Barnard 29, and Moehler et al. (1998) and Thompson et al. (2006) for ROA 5701. However, absolute abundances may contain systematic errors, due, for example, to inaccuracies in the atmospheric parameters and atomic data, in particular the *f*-values. In order to minimize these errors, a detailed line-by-line differential abundance analysis can be performed, with respect to a young B-type star of known chemical composition (Population I) which has similar atmospheric parameters. Therefore, in Table 5 the abundances of Barnard 29 and ROA 5701 are compared to those of young B-type stars in the Galactic cluster NGC 6611 (Hunter et al. 2007) and in the local field (Kilian 1992, 1994). For the former, results have been determined using the same non-LTE model atmosphere calculations as in the present paper. The latter uses different model atmosphere calculations and hence differential abundances using this source may not be as reliable. The standard error in the differential abundance estimates for Barnard 29 and ROA 5701, as compared with young B-type stars, are typically ± 0.2 dex. These errors do not include any systematic errors due to the atmospheric parameters as these are assumed to cancel due to the use of the same methods for both samples. Note that where we did not have access to results for individual absorption lines, differential abundance values are based on the mean abundance estimates listed, with a minimum error of ± 0.2 dex.

It is not possible to perform a differential analysis for Fe III UV lines using young B-type stars, as these are affected by line crowding and are often saturated. The strengths of the Fe III absorption lines are only weakly dependent on the effective temperature and surface gravity, so they should not be a significant source of error. In order to test the dependence on microturbulence for young B-type stars, the Galactic star HR 1886 was examined using STIS spectra taken from the *HST* archive. This star was chosen as its $T_{\rm eff} = 24\,000$ K and $\log g = 4.1$ dex (Hambly et al. 1996) are similar to those of ROA 5701. For a microturbulence of 0 km s^{-1}, synthetic spectra were generated and scaled to the same mean flux as the observed spectrum, using the methods described in Section 3.4. The microturbulence was then increased to 10 km s^{-1}, and the process repeated. The change in microturbulence resulted in a change of metallicity of $\sim$1.4 dex, implying that Fe III UV lines in Galactic B-type stars

Table 5. Differential abundances for Barnard 29 and ROA 5701, relative to those in young B-type stars from Hunter et al. (2007) where available, supplemented by Kilian (1992, 1994)†. Also listed are differential abundances relative to the ISM values (Cardelli et al. 1996; Snow & Witt 1996; Meyer et al. 1997, 1998; Wilms et al. 2000), and the metallicities of M 13◇ (Yong et al. 2006) and ω Cen★ (Origlia et al. 2003).

Species	Young B-type stars							ISM	
	Barnard 29				ROA 5701			Barnard 29	ROA 5701
	This paper	Con 94	Dix 98	Moe 98	This paper	Moe 98	Tho 06	This paper	
C	<-1.3	<-1.3	-1.8	–	<-1.4	<-2.1	<-1.4	<-1.7	<-1.8
N	-0.3	-0.3	–	–	-0.6	-0.7	-0.6	-0.5	-0.8
O	-1.1	-1.0	–	–	-0.8	-0.6	-0.8	-1.2	-0.9
Mg	-1.2	-1.3	–	–	-1.2	–	-1.1	-1.3	-1.3
Si	-1.0	-1.1	–	–	-1.2	-1.3	-1.5	-0.8	-1.1
Al†	-1.1	-1.0	–	–	<-1.4	–	<-1.0	-1.2	<-1.5
S†	-1.5	<-1.0	-1.9	–	-1.6	–	-1.5	-1.4	-1.5
Fe (Optical)	-1.4	<-0.8	–	–	<-1.4	–	–	-1.4	<-1.4
Fe (UV)	-2.1	–	-2.2	-2.2	-2.4	-2.7	–	-2.1	-2.1
Cluster [Fe/H]		-1.6◇				-1.6★			

Note: Con 94 = Conlon et al. (1994), Dix 98 = Dixon & Hurwitz (1998), Moe 98 = Moehler et al. (1998), Tho 06 = Thompson et al. (2006).

are indeed very sensitive to changes in microturbulence, and are not appropriate for a differential abundance analysis.

Kendall et al. (1994a) found a similar dependence on microturbulence for the standard star HD 149438 (τ Scorpii), with a change of ξ from 0 to 10 km s^{-1} yielding a metallicity change of $\sim$0.8 dex. For Barnard 29 and ROA 5701, a ξ change from 0 to 10 km s^{-1} resulted in a metallicity change of $\sim$0.4 and 0.2 dex, respectively.

4.2.1 *Barnard 29*

Differential abundances for Barnard 29, relative to young B-type stars, are given in Table 5, along with the results of Conlon et al. (1994), Dixon & Hurwitz (1998) and Moehler et al. (1998). As stated previously, Conlon et al. (1994) used *IUE* and WHT/UES data with LTE models in their analysis. Their upper limit for the C abundance agrees with that found in this paper, while N, O, Mg, Si and Al are $\sim$0.1 dex lower. Reasons for the differences in abundance could include different atmospheric parameters, improved equivalent width measurements (as a consequence of our higher S/N observations), and our use of non-LTE model atmosphere codes. To investigate if our non-LTE treatment may be responsible for the differences, we have calculated LTE abundances for the elements, with the exception of Al which is already in LTE. This results in abundances of $<$5.93 for C, 7.40 dex for N, 7.75 dex for O, 5.93 dex for Mg and 6.78 dex for Si. The N, O and Si abundances are still larger than the Conlon et al. (1994) abundances, while C and Mg are lower.

The lower microturbulence used in the present analysis may be a further source of the differences. Adopting a microturbulence of 10 km s^{-1} from Conlon et al. (1994), LTE abundances of 7.30 dex for N, 7.62 dex for O and 6.47 dex for Si are obtained, while the other elements abundances do not significantly change. The values are now in good agreement with Conlon et al. (1994), with the exception of C, suggesting that the microturbulence is a factor. The discrepancy for C may be due to the use of different lines. However, the results in the present paper should be more reliable due to our use of non-LTE techniques and improved observational data.

Dixon & Hurwitz (1998) used a far-UV spectrum from *ORFEUS-SPAS II*, fitting LTE synthetic models to the data, similar to the method used here. They determined abundances for the elements He, N, O, Al and S, finding results consistent with Conlon et al. (1994) but with larger error bars, suggesting the use of lower resolution data as the reason for this. The C abundance of Dixon & Hurwitz (1998) was found using two C III lines, and is $-$0.5 dex lower than the upper limit found here. Their S abundance was derived from lines of S III and S IV, with some scatter due to blending with nearby features. These authors also observed S II lines, but these were not included in the analysis as they appeared to be affected by non-LTE. The S abundance of Dixon & Hurwitz (1998) is $\sim$0.4 dex lower than our value, which may be due to the use of different spectral wavelength regions.

An iron abundance of [Fe/H] $= -2.2$ was determined by both Dixon & Hurwitz (1998) and Moehler et al. (1998). Dixon & Hurwitz (1998) found it difficult to determine an Fe abundance, as the spectrum was contaminated by interstellar lines and many of the expected Fe transitions were in regions of poorly fitted continuum. They fitted a band of Fe lines rather than individual features, similar to the method used in this paper for the UV observations, noting that their abundance was more than 0.5 dex below the model atmosphere used to derive the synthetic spectra (i.e. [M/H] $= -1.5$), with tests showing that the model choice had little effect on the abundance. Moehler et al. (1998) determined an Fe abundance using the same GHRS/*HST* spectrum employed here. They adopted the atmospheric parameters of Conlon et al. (1994), and fitted a global continuum to the normalized data, noting that an uncertainty of 5 per cent in the continuum definition of their spectrum would lead to an error of 0.2 dex in the derived abundance.

In the present paper, an Fe III abundance of [Fe/H] $= -2.1$ is obtained from the UV spectrum and [Fe/H] $= -1.4$ from the optical. The UV value is well below the metallicity of the cluster ([Fe/H] $= -1.6$, Yong et al. 2006), but is in slightly better agreement compared to the previous UV studies. However, our optical result is consistent with the cluster metallicity, to within the errors. This discrepancy is discussed further in Section 4.4.

4.2.2 *ROA 5701*

For ROA 5701, there is good agreement between the present abundances and those of Thompson et al. (2006), with C, N and O giving the same differential values. The Si abundance estimates differ by 0.2 dex, and this discrepancy appears to be due to differences in the atmospheric parameters. This was tested by calculating non-LTE abundances using the equivalent widths from this paper and the atmospheric parameters from Thompson et al. (2006). The resulting values are 5.93 dex for Si III and 5.88 dex for Si IV, suggesting the changed atmospheric parameters are a cause for the differences.

The upper limit to the C abundance of Moehler et al. (1998) is lower than that derived in this paper, despite using the same upper limit value for the equivalent width. This difference could be due to large non-LTE effects in C II, as proposed by Sigut (1996) and hence, the upper limit derived here may be more reliable. Although the N and O abundances of Moehler et al. (1998) differ by $\sim$0.2 dex, and the Si abundance by $\sim$0.1 dex, from those presented here, again this may be due to non-LTE effects. To test this, LTE abundances have been derived, using the TLUSTY grid, resulting in $<$6.23 dex for C, 7.99 dex for O, 7.10 dex for N and 6.50 dex for Si. The O abundance is in very good agreement with Moehler et al. (1998), but the C, N and Si values are still higher. The changes could be due to the use of different equivalent width measurements and atmospheric parameters. However, the present results should be more reliable due to our non-LTE analysis.

No abundances for Mg, Al or S were derived by Moehler et al. (1998), while Thompson et al. (2006) determined values for Mg and S, which differ from those found in this paper by $\sim$0.1 dex. This is probably due to the improved S/N observations, which allow better equivalent width measurements; changing the atmospheric parameters had little effect on these abundances. The listed Al abundance is still an upper limit, but due to the improved S/N of the spectrum it was possible to place a revised lower limit on the equivalent width. In general, the abundances quoted in the present paper should be more accurate due to the improved quality of the observational data.

Thompson et al. (2006) observed two unidentified features at 4512.41 and 4352.22 Å in their data, which were obtained using UCLES at the AAT. However, no features are observed at these wavelengths in the FEROS spectrum, which is of higher resolution and S/N, indicating that the lines in the UCLES data may not be real.

Moehler et al. (1998) obtained a differential Fe III abundance of [Fe/H] $= -2.7$ from the GHRS/*HST* UV spectrum, compared to [Fe/H] $= -2.4$ derived here. Both values are lower than the metallicity of ω Cen, namely [Fe/H] $= -1.6$ (Origlia et al. 2003), although our result is in better agreement with the metallicity of the cluster.

Table 6. Absolute abundances for Barnard 29 and ROA 5701 from their optical spectra. Also tabulated are the abundances of the M 13 giants (Cohen & Meléndez 2005[a] and Yong et al. 2006) and those of ω Cen, using the main cluster giant population (Smith et al. 2000[b] and Origlia et al. 2003).

Species	M 13		ω Cen	
	Barnard 29	Giants	ROA 5701	Giants
C	<6.64	–	<6.54	6.86
N	7.45	–	7.06	–
O	7.50	7.53	7.76	7.45
Mg	6.10	6.14	6.15	6.26
Si	6.45	6.38	6.17	6.26
Al	5.14	5.75[a]	<4.87	4.87[b]
S	5.72	–	5.62	–
Fe	6.07	5.90	<6.02	5.92

An optical value [Fe/H] < -1.4 is obtained in the present paper. The [Fe/H] abundance of ROA 5701 is discussed further in Section 4.4.

4.3 Comparison with Cluster Giants

The absolute abundances of Barnard 29 and ROA 5701 are given in Table 6, along with those of giants from their respective clusters, namely M 13 (Cohen & Meléndez 2005; Yong et al. 2006) and ω Cen (Smith et al. 2000; Origlia et al. 2003). In general the abundances compare well, to within the errors. A notable exception is the Al abundance of Barnard 29, which is lower than that of the giants. However, Yong et al. (2006) and Sneden et al. (2004) have both shown that the aluminium abundances in the giants range from [Al/Fe] $\sim$ 0–1.2 dex. The giants with [Al/Fe] $\sim$ 0.3 have similar O abundances to those found here, suggesting that the Barnard 29 abundance compares well with a selection of the giant population.

4.4 Evolutionary discussion

4.4.1 Dredge-up

Thompson et al. (2006) previously studied ROA 5701, suggesting that the observed abundance patterns implied that the star had left the AGB prior to the onset of the third dredge-up, as have Conlon et al. (1994) to similarly explain the abundance patterns in Barnard 29. Dredge-up occurs in stars during their AGB evolution, as products of hydrogen and helium burning are moved from the core to the surface, altering the surface composition (Iben & Renzini 1983). Briefly, during the first dredge-up, the surface O sees little change while C decreases as N increases. The second dredge-up sees C and O mostly converted into N. At the third dredge-up, triple-α products are brought to the surface and C is enhanced relative to O and N.

Both Barnard 29 and ROA 5701 exhibit abundance patterns compatible with no third dredge-up. The N abundances are strongly enhanced relative to both C and O, especially for Barnard 29, while O is larger than C. This is consistent with the previous studies of both stars, with the exception of the lower N abundance of Moehler et al. (1998) for ROA 5701. Thus the abundances of CNO appear compatible with the suggestion that the third dredge-up may not have occurred.

The low C abundance could be explained in terms of hot bottom burning (HBB). Deroo et al. (2005) found V435 Oph to have a low metallicity and no enhancement of C, suggesting HBB as an explanation of the observed abundances. In HBB (Mooney et al. 2001), C is converted to N at the base of the convective envelope, when temperatures become large enough for CNO processing. Herwig (2005) indicates that HBB may have an important role at extremely low metallicities. However, D'Antona & Mazzitelli (1996) suggest that Population I stars of initial mass $M \geqslant 5\,\mathrm{M}_{\odot}$, and Population II stars of $M \geqslant 3.5\,\mathrm{M}_{\odot}$ experience HBB. As the initial mass of the stars is unknown, no conclusions can be made regarding this process.

4.4.2 Gas–dust separation

Although the lack of a third dredge-up appears a likely explanation for the abundance patterns of the light elements in both stars, Moehler et al. (1998) and Dixon & Hurwitz (1998) explain the abundances of the heavier elements in terms of the gas–dust separation process. The basic premise involves grain formation that occurs in the circumstellar shells of stars during the AGB evolution. Dust particles are removed by radiation pressure and the 'cleaned' gas is re-accreted on to the surface (Mathis & Lamers 1992; Waters et al. 1992). This results in abundances similar to the ISM, that is, CNO and S near solar, while other elements such as Mg, Al, Si and Ca follow the low Fe abundance (Van Winckel et al. 1995) and see, for example, the RV Tauri stars UY CMa, HP Lyr and BZ Sct (Giridhar et al. 2005). Parthasarathy, Garcia Lario & Pottasch (1992) found that, in the atmospheres of post-AGB stars, metals with a high condensation temperature, for example, Fe, are more likely to condense into dust grains, compared to elements such as C, N, O and S with low condensation temperatures which stay in the gas phase with no significant depletions observed.

Moehler et al. (1998) suggested that this process occurred as they found a low Fe value, with N and O virtually undepleted, while Dixon & Hurwitz (1998) also cite the low Fe abundance as evidence for the process. For this scenario, similar depletions of Mg, Si and Fe would therefore be expected. Examining the differential ISM abundances (Table 5) it is possible to determine if the stars follow the abundance trends seen in gas–dust separation. For Barnard 29, we find differential abundances of [Mg/H] $= -1.3$, [Al/H] $= -1.2$, [Si/H] $= -0.8$, [S/H] $= -1.4$ and [Fe/H] (optical) $= -1.4$ (relative to the ISM). In addition, for ROA 5701 the differential abundances are [Mg/H] $= -1.3$, [Si/H] $= -1.1$ and [S/H] $= -1.5$. The Mg, Al and Fe (optical) abundances of Barnard 29 agree with the value for S and the metallicity and giant abundances of M 13 ([Fe/H] $= -1.6$, Yong et al. 2006), although the Si abundance estimate is somewhat larger, possibly due to its sensitivity to the atmospheric parameters. For ROA 5701, the S abundance agrees (to within the errors) with the Mg and Si values and is consistent with the metallicity and giants of ω cen ([Fe/H] $= -1.6$, Origlia et al. 2003). Similar results would be obtained if the abundances were compared with young B-type stars instead of the ISM.

For gas–dust separation, CNO and S would be expected to be relatively undepleted and not in agreement with Mg, Si, Al or Fe. However, we find that the S abundance is generally in agreement with the Mg, Si, Al and Fe (optical) abundances, suggesting that gas–dust separation has not occurred. Also this process is generally confined to binary systems. The possible binarity of our two stars was investigated using radial velocity measurements. However, a literature search produced sparse results, indicating no conclusions can be made. Additionally, the position of the stars on log g/T_{eff} or log L/T_{eff} diagrams (Conlon et al. 1994; Blöcker 1995) suggest core masses for both stars of $\sim$0.55 $\mathrm{M}_{\odot}$, using $\log(L/\mathrm{L}_{\odot}) = 3.2$

(Landsman et al. 1992) for ROA 5701 and $\log(L/L_{\odot}) = 3.23$ (Adelman et al. 1994) for Barnard 29. Conlon et al. (1993) found that stars of this average mass do not show an infrared excess, which is supported by the lack of *IRAS* detection for both stars, and no emission features observed in Hα for ROA 5701. These results suggest there is no evidence of a circumstellar dust shell present for either star. Hence the gas–dust separation process appears unlikely to be responsible for the observed abundance patterns.

4.4.3 *UV lines*

In this paper, we find a difference of 0.7 dex and <1.0 dex for Barnard 29 and ROA 5701, respectively, between the optical and UV derived iron abundances. Analyses of the Fe III lines in other hot post-AGB stars, such as BD +33°2642 (Napiwotzki, Heber & Köppen 1994) and HD 177566 (Kendall et al. 1994a,b), show similar Fe abundance trends to those found here. Napiwotzki et al. (1994) analysed optical and *IUE* spectra, and their results led them to suggest the occurrence of gas–dust separation, as He was near solar, C, N, O, Mg and Si depleted by ∼1.0 dex, and Fe depleted by ∼2.0. Kendall et al. (1994b) set upper limits for the Fe abundance from Fe III lines in both optical and UV spectra, finding a difference of ∼0.5 dex between the two sets of data. Similarly, Moehler et al. (1998) derived an Fe abundance of [Fe/H] = 6.95 dex from the Fe III lines in the *IUE* spectra of the main-sequence B-type star γ Peg, compared to [Fe/H] = 7.56 dex from optical Fe III transitions. In addition, Grigsby, Mulliss & Baer (1996) in their analysis of ι Her found that the UV Fe abundance was $\geqslant$0.5 dex below the near solar value derived from optical lines. Gies & Lambert (1992) and Proffitt & Quigley (2001) studied the B-type supergiant HD 51309. While the former state two different iron abundance estimates depending on the temperature structure used, there is a difference of $\geqslant$0.75 dex found between their optical results (from Fe II and Fe III lines) and the *IUE* iron abundance of Proffitt & Quigley (2001).

Dufton (in preparation) have observed similar abundance discrepancies for young B-type stars in the SMC and LMC, as well as in the Magellanic Bridge (MB). They determined Fe abundances from GHRS/*HST* and STIS/*HST* spectra, using the same methods and Fe III transitions as described here, and found that these were consistently lower (more than 0.5 dex) than the estimated metallicities of the SMC, LMC and MB regions.

It is possible to derive the abundance of other elements using UV spectra, but that is not possible here as the GHRS data employed do not cover a large enough spectral range. However, *IUE* spectra have been used by a number of authors to derive the abundances of several light elements. Conlon et al. (1991) obtained a C abundance using both UV and optical spectra, finding the abundances to be compatible. Kendall et al. (1994b) found similar differential abundances for C, N and Si between their optical and *IUE* spectra, with differences being less than 0.15 dex. Also, the Mg abundance obtained by Napiwotzki et al. (1994) showed a difference of 0.05 dex between their optical and UV values. However, the UV abundances obtained by Napiwotzki et al. (1994) for C and S are lower by 0.5 and 0.4 dex, respectively, than the optical abundances determined here (see Section 4.2.1). Despite this result, the use of UV spectra to determine the abundances of light elements generally appears to be reliable and do not suffer the same problem observed with iron.

4.4.4 *Oscillator strengths*

The above studies, in conjunction with the present work, strongly indicate that the UV Fe III lines yield systematically low Fe abundances, possibly as a result of errors in the adopted atomic data, in particular *f*-values. Currently, atomic data from Kurucz models (http://nova.astro.umd.edu; Hubeny 1988; Hubeny & Lanz 1995; Hubeny et al. 1998) are used in the TLUSTY grids. We have therefore performed a literature search of *f*-values for Fe III, to investigate if more recent calculations or measurements would produce different Fe abundances. Table 7 lists the six strongest transitions observed in the GHRS/*HST* spectra, along with the oscillator strengths from Kurucz, and the more recent results of Nahar & Pradhan (1996) and Toner & Hibbert (2005). There are little differences between the sets of atomic data, so these will not solve the Fe abundance problem. However, we note that further calculations and measurements for these Fe III transitions are planned in the future.

Despite numerous studies of the UV Fe III transitions, the line list for the spectral region employed in this paper may not be complete. However, it is assumed that, if this is the case, any lines excluded during the fitting procedure would be compensated by making other transitions too strong. This would potentially lead to an overestimate in the derived abundance, which would not solve the abundance discrepancy observed.

4.4.5 *Further work*

To investigate the Fe abundance discrepancy further will require very high-S/N data for Barnard 29 and ROA 5701, sufficient to ascertain the reliability of the observed optical Fe III lines and observe further Fe III lines in both stars. Unlike the UV transitions, the optical lines are sufficiently weak, even in main-sequence Population I B-type stars, for a detailed line-by-line differential abundance analysis to be performed. This will hence allow the removal of systematic effects such as the dependence on *f*-value, and hence the determination of accurate Fe abundances, for comparison with the UV measurements. We plan such observations in the near future.

Table 7. Strongest transitions of Fe III seen in the UV spectra of Barnard 29 and ROA 5701. Oscillator strengths are taken from Kurucz, Nahar & Pradhan (1996)[a] and Toner & Hibbert (2005).

Transition[a]	g_i[a]	g_j[a]	Wavelength (Å)	log *gf* values		
				Kurucz	Nahar & Pradhan (1996)	Toner & Hibbert (2005)
a^5G^e–z^5F^o	5	5	1869.841	−0.666	−0.672	–
a^5G^e–z^5F^o	5	3	1871.152	−0.121	−0.116	–
b^5D^e–y^5D^o	9	9	1877.990	0.238	0.273	–
a^5G^e–z^5F^o	13	11	1890.664	0.434	0.407	–
a^7S^e–z^7P^o	7	9	1895.456	0.461	0.415	0.436
a^3I^e–y^3H^o	13	11	1896.814	0.480	0.398	–

5 CONCLUSIONS

The abundance patterns observed for both Barnard 29 and ROA 5701 indicate that the stars have not undergone the third dredge-up. In addition, the gas–dust separation process suggested by previous authors appears unlikely. The optical spectra imply abundances for the Fe and other elements, which are compatible with those found in the late-type giants, while the Fe III lines in the UV produce lower abundances than expected, as found in several other studies. This strongly suggests that the UV Fe III do not provide reliable abundance indicators. Future studies require high-S/N optical data, in order to obtain accurate Fe abundance estimates. A re-evaluation of the Fe III *f*-values, either theoretically or experimentally, would also be highly desirable.

ACKNOWLEDGMENTS

Some of the data presented in this paper were obtained from the Multimission Archive at the Space Telescope Science Institute (MAST). STScI is operated by the Association of Universities for Research in Astronomy, Inc., under NASA contract NAS5-26555. Support for MAST for non-*HST* data is provided by the NASA Office of Space Science via grant NAG5-7584 and by other grants and contracts. IRAF is distributed by the National Optical Astronomy Observatories, USA. We would like to thank Ian Howarth for his continued help. HMAT acknowledges financial support from the Northern Ireland Department of Education and Learning (DEL). FPK is grateful to AWE Aldermaston for the award of a William Penney Fellowship. JVS thanks the staff of the McDonald observatory for their expert assistance in taking these observations and the Particle Physics and Astronomy Council for financial support. DLL thanks the Robert A. Welch Foundation of Houston, Texas for their support. AAZ thanks the SAAO for hospitality during a sabbatical visit.

REFERENCES

Adelman S. J., Aikman G. C. L., Hayes D. S., Philip A. G. D., Sweigart A. V., 1994, A&A, 282, 134
Auer L. H., Norris J., 1974, ApJ, 194, 87
Barnes J., 1993, A Beginner's Guide to Using IRAF. NOAO Laboratory, Tuscon, AZ
Blöcker T., 1995, A&A, 299, 755
Cacciari C., Caloi V., Castellani V., Fusi Pacci F., 1984, A&A, 139, 285
Cardelli J. A., Meyer D. M., Jura M., Savage B. D., 1996, ApJ, 467, 334
Cheng Y.-S., Chang R.-C., 2000, Appl. Opt., 39, 4058
Cohen J. G., Meléndez J., 2005, ApJ, 129, 303
Conlon E. S., Dufton P. L., Keenan F. P., McCausland R. J. H., 1991, MNRAS, 248, 820
Conlon E. S., Dufton P. L., Keenan F. P., McCausland R. J. H., Little J. E., 1993, A&A, 272, 243
Conlon E. S., Dufton P. L., Keenan F. P., 1994, A&A, 290, 897
D'Antona F., Mazzitelli I., 1996, ApJ, 470, 1093
de Boer K. S., 1985, A&A, 142, 321
Deroo P., Reyniers M., Van Winckel H., Goriely S., Siess L., 2005, A&A, 438, 987
Dixon W. V., Hurwitz M., 1998, ApJ, 500, L29
Dufton P. L., Ryans R. S. I., Trundle C., Lennon D. J., Hubeny I., Lanz T., Allende Prieto C., 2005, A&A, 434, 1125
Dufton P. L., Ryans R. S. I., Simón-Díaz S., Trundle C., Lennon D. J., 2006, A&A, 451, 603
Gies D. R., Lambert D. L., 1992, ApJ, 387, 673
Giridhar S., Lambert D. L., Reddy B. E., Gonzalez G., Yong D., 2005, ApJ, 627, 432
Grevesse N., Sauval A. J., 1998, Space Sci. Rev., 85, 161
Grigsby J. A., Mulliss C. L., Baer G. M., 1996, PASP, 108, 953
Hambly N. C., Keenan F. P., Dufton P. L., Brown P. J. F., Saffer R. A., Peterson R. C., 1996, ApJ, 466, 1018
Harris H. G., Nemec J. M., Hesser J. E., 1983, PASP, 95, 256
Harris W. E., 1996, AJ, 112, 1487
Herwig F., 2005, ARA&A, 43, 435
Howarth I. D., Murray J., Mills D., Berry D. S., 2004, Starlink User Note 50.24: DIPSO – A Friendly Spectrum Analysis Program. Rutherford Appleton Laboratory/CCLRC, Didcot
Hubeny I., 1988, Comput. Phys. Commun., 52, 103
Hubeny I., Lanz T., 1995, ApJ, 439, 875
Hubeny I., Heap S. R., Lanz T., 1998, in Boulder-Munich, II, Howarth I. D., eds, ASP Conf. Ser. Vol. 131., Properties of Hot, Luminous Stars. Astron. Soc. Pac., San Francisco, p. 108
Hunter I., Dufton P. L., Ryans R. S. I., Lennon D. J., Rolleston W. R. J., Hubeny I., Lanz T., 2005, A&A, 436, 687
Hunter I. et al., 2007, A&A, 466, 277
Iben I. Jr, Renzini A., 1983, ARA&A, 21, 271
Kaufer A., Stahl O., Tubbesing S., Norregaard P., Avila G., Francois P., Pasquini L., Pizzella A., 1999, The Messenger, 95, 8
Kendall T. R., Conlon E. S., Dufton P. L., Keenan F. P., 1994a, A&A, 290, 563
Kendall T. R., Brown P. J. F., Conlon E. S., Dufton P. L., Keenan F. P., 1994b, A&A, 291, 851
Kilian J., 1992, A&A, 262, 171
Kilian J., 1994, A&A, 282, 867
Kwok S., ARA&A, 1993, 31, 63
Landsman W. B. et al., 1992, ApJ, 395, L21
Landsman W., Moehler S., Napiwotzki R., Heber U., Sweigart A., Catelan M., Stecher T., 2000, in Leige, Noels A., Magain P., Caro D., Jehin E., Parmentier G., Thoul A. A., eds, 35th Leige Int. Astrophys. Colloq., The Galactic Halo: From Globular Cluster to Field Stars. Inst. d'Astrop. et de Geop., Belgium, p. 515
Lee J.-K., Rolleston W. R. J., Dufton P. L., Ryans R. S. I., 2005, A&A, 429, 1025
Lehner N., Dufton P. L., Lambert D. L., Ryans R. S. I., Keenan F. P., 2000, MNRAS, 314, 199
Mathis J. S., Lamers H. J. G. L. M., 1992, A&A, 259, L39
Meyer D. M., Cardelli J. A., Sofia U. J., 1997, ApJ, 490, L103
Meyer D. M., Jura M., Cardelli J. A., 1998, ApJ, 493, 222
Moehler S., 2001, PASP, 113, 1162
Moehler S., Heber U., Lemke M., Napiwotzki R., 1998, A&A, 339, 537
Mooney C. J., Rolleston W. R. J., Keenan F. P., Dufton P. L., Pollacco D. L., Magee H. R., 2001, MNRAS, 326, 1101
Mooney C. J., Rolleston W. R. J., Keenan F. P., Dufton P. L., Smoker J. V., Ryans R. S. I., Aller L. H., Trundle C., 2004, A&A, 419, 1123
Nahar S. N., Pradhan A. K., 1996, A&AS, 119, 509
Napiwotzki R., Heber U., Köppen J., 1994, A&A, 292, 239
Nieva M. F., Przybilla N., 2006, ApJ, 639, L39
Norris J., 1974, ApJ, 194, 109
Oudmaijer R. D., 1996, A&A, 306, 823
Origlia L., Ferraro F. R., Bellazzini M., Pancino E., 2003, ApJ, 591, 916
Parthasarathy M., Garcia Lario P., Pottasch S. R., 1992, A&A, 264, 159
Proffitt C. R., Quigley M. F., 2001, ApJ, 548, 429
Ryans R. S. I., Dufton P. L., Rolleston W. R. J., Lennon D. J., Keenan F. P., Smoker J. V., Lambert D. L., 2002, MNRAS, 336, 577
Ryans R. S. I., Dufton P. L., Mooney C. J., Rolleston W. R. J., Keenan F. P., Hubeny I., Lanz T., 2003, A&A, 401, 1119
Savage B. D., Sembach K. R., 1996, ARA&A, 34, 279
Sigut T. A. A., 1996, ApJ, 473, 452
Smith V. V., Suntzeff N. B., Cunha K., Gallino R., Busso M., Lambert D. L., Straniero O., 2000, ApJ, 119, 1239
Sneden C., Kraft R. P., Guhathakurta P., Peterson R. C., Fulbright J. P., 2004, ApJ, 127, 2162
Snow T. P., Witt A. N., 1996, ApJ, 468, L65
Toner A., Hibbert A., 2005, MNRAS, 364, 683
Thompson H. M. A., Keenan F. P., Dufton P. L., Ryans R. S. I., Smoker J. V., 2006, MNRAS, 368, 1749

Trundle C., Dufton P. L., Rolleston W. R. J., Ryans R. S. I., Lennon D. J., Lehner N., 2001, MNRAS, 328, 291
Tull R., MacQueen P. J., Sneden C., Lambert D. L., 1995, PASP, 107, 251
Valdes F., 1993, Guide to the Slit Spectra Reduction Task DOECSLIT. NOAO Laboratory, Tuscon, AZ
Van Winckel H., 2003, ARA&A, 41, 391
Van Winckel H., Waelkens C., Waters L. B. F. M., 1995, A&A, 293, L25
Waters L. B. F. M., Trams N. R., Waelkens C., 1992, A&A, 262, L37
Wilms J., Allen A., McCray R., 2000, ApJ, 542, 914
Yong D., Aoki W., Lambert D. L., 2006, ApJ, 638, 1018
Zinn R. J., Newell E. B., Gibson J. B., 1972, A&A, 18, 390

This paper has been typeset from a TEX/LATEX file prepared by the author.